Soft Matter

Accepted Manuscript

ROYAL SOCIETY OF CHEMISTRY

www.rsc.org/softmatter

Soft Matter

Soft Matter

Dynamic Article Links ►

Cite this: DOI: 10.1039/c0xx00000x

www.rsc.org/xxxxxx

FULL PAPER

Geometric Reconstruction of Biological Orthogonal Plywoods

Oscar F. Aguilar Gutierrez*[a] and Alejandro D. Rey*[a]

Received (in XXX, XXX) Xth XXXXXXXXX 20XX, Accepted Xth XXXXXXXXX 20XX
DOI: 10.1039/b000000x

In this paper we focus on structure determination of biological orthogonal plywoods, fiber-like composite analogues of liquid crystalline phases, where the fibrils of the building blocks show sharp 90° orientation jumps between fibers in adjacent domains. We present an original geometric and computational modelling that allows to determine the fibrillary orientation in biological plywoods from periodic herringbone patterns commonly observed in cross-sections. Although herringbone patterns were long reported, the specific and quantitative relations between herringbones and the orthogonal plywoods were absent or at best incomplete. Here we provide an efficient and new procedure to perform an inverse problem that connects two specific features of the herringbone patterns (aperture angle and wavelength) with the 3D morphology of the structure, whose accuracy and validity was ascertained through *in-silico* simulations and also with real specimens ("Eremosphera viridis"). This contribution extends significantly the better known characterization methods of 2D cross sections, such as the arced patterns observed in biological helicoidal plywoods, and with the present proposed methodology it adds another characterization tool for a variety of biological fibrous composites that form cornea-like tissues.

1. Introduction

Ordered structures found throughout Nature show a variety of architectures consisting of fibrillar building blocks such as collagen in vertebrates, cellulose in plants and chitin in insects, and are formed through an efficient entropy-driven self-assembly process [1, 2, 3]. The relationship between the architecture of these fiber-based structures and the functionalities such as mechanical behaviour, optical properties is widely recognized [4, 5], yet poorly understood, and has become a source of inspiration in the last decades which has influenced the development of new materials [2, 6, 7, 8].

Biological liquid crystals are commonly observed in sufficiently stiff fibril-based materials and are classified into: (i) solid analogues, (ii) in-vitro biopolymer solutions, and (iii) in-vivo materials and secretions. The current paper focuses on solid analogues; the reader is referred to [1, 2, 9 & 10] for more information regarding in vivo and in vitro liquid crystals. Solid analogues or biological plywoods (referred hereupon as plywoods) are materials that present a frozen-in orientated ordered structure from a previous self-assembly step involving liquid crystal organization [11, 12]. Common types of plywoods are nematic, helical and orthogonal and are described in detail in Fig. 1 together with key geometric quantities and expected cross-sectional patterns. In nematics, the fibrils show a single preferred orientation (a-c), and cross-sections give line (c) or dot (b) patterns. In helicoids, the fibrils rotate continuously in the normal direction (e-f) to parallel planes on a periodic distance p_o known as the pitch and cross-sections display helical (e) or arced patterns (f). In orthogonal plywoods, the fibers display a homogeneous domain structure with a sharp fiber rotation between domains (h-g-i) and cross-section are dot-line (h), line-line (i), or herringbone (g) patterns. The plywoods showing a helicoid (d) display the organization of cholesteric liquid crystals or chiral nematics N*, and its abundance in plants and insects is associated with mechanical property optimization that removes the disadvantages of anisotropy as well as diffraction functionalities, as in beetles [13, 14] and tulips [15, 16]. Given the functional versatility and widespread presence in plants and insects, helicoids have been intensely studied [1, 8, 10 & 17].

The structure characterization of biological fibrous composites involves determining the fiber orientation and chiral pitch or domain scales and is a complex inverse problem usually approached using optical methods [18, 19] or by sectioning samples and then performing an analysis based on the resulting 2D cross-sectional patterns shown in Figure 1. As mentioned above, cross-sectional patterns of helicoids are usually periodic arced patterns of maximum curvature κ_{max} while cross-sections of orthogonal plywoods are herringbone patterns with an aperture angle β. Figure 2 shows a schematic of main geometric features of the arc patterns-helicoids and herringbone patterns-orthogonal plywoods. The reconstruction, indicated by the thick arrows, involves converting the geometric information of these 2D patterns into the full 3D structure. It is crucial to note the 2D patterns are sensitive to the slicing angle α and not all slicing angle produce these distinctive patterns, as further discussed in section 1.1. Hence a quantitative understanding of the relation between the pattern and the slicing angle α is crucial. Techniques for ideal and complex arced patterns have been presented [20, 21] and validated [14] but

Cite this: DOI: 10.1039/c0xx00000x

www.rsc.org/xxxxxx

FULL PAPER

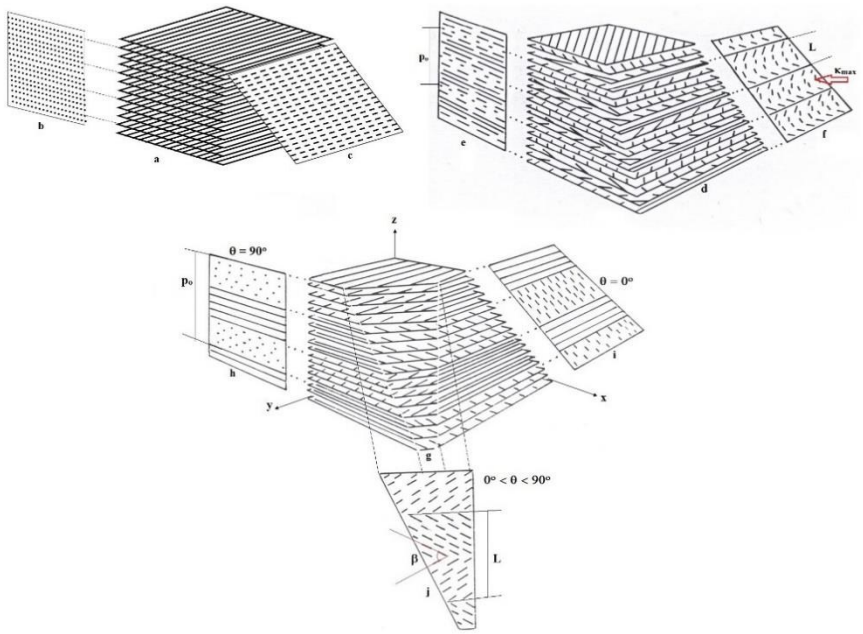

Fig. 1 Schematic representation of a nematic plywood (a-c) as a series of planes with parallel alignment throughout the entire structure (a) with projections corresponding to dots (b) when the incision is orthogonal to the fibril alignment and a sequence of parallel lines (c) with any other incision angle; helicoidal plywoods (d-f) where the cholesteric arrangement of pitch p_o is shown (d) and projections corresponding to periodic structures but no arced patterns with periodicity $p_o/2$ (e) and the arced patterns with oblique incisions of periodicity L and maximum curvature κ_{max} (f); and the orthogonal plywood (g-j) showing several layers orthogonally arranged and projections without any distinguishable pattern when the incision is aligned with one of the fibril orientation (h-i) and the herringbone patterns of periodicity L and aperture angle β, with a rotation of the oblique incisions.

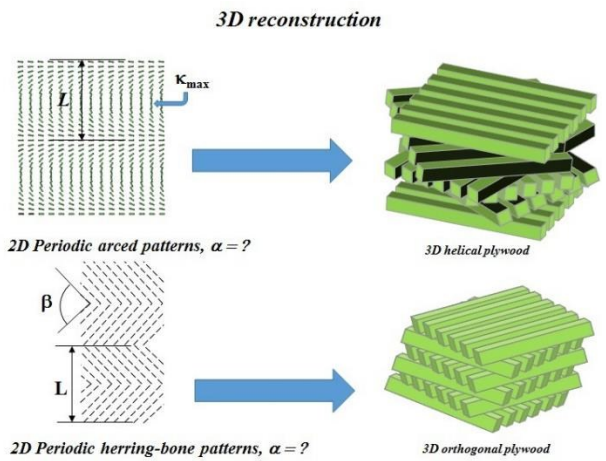

Fig. 2 Summary of the cross-sectioning characterization procedures, where the full 3D helical and orthogonal structures are reconstructed from 2D observations from the periodic arced patterns [26] and herringbone patterns (this work). The periodic arc-patterns have a 2D periodicity L and maximum curvature κ_{max}. The periodic herringbone patterns have periodicity L and aperture angle β. In both case the slicing angle α is unknown.

herringbone patterns remain largely unexplored.

The objective of this paper is to present and validate a methodology for structure characterization of orthogonal plywoods from geometric modelling of 2D herringbone patterns. The ill-conditioning of inverse problems is adequately overcome in this approach by developing an error sensitivity analysis based on in-silico herringbones generated by a versatile 3D visualization method for arbitrary orientation vector fields. This article is organized as follows. Section 1.1 presents a brief discussion of biological plywoods, fibrillar arrangements, and characteristic 2D patterns on cross-sections. Section 2.1 presents the geometric model that forms the basis of converting herringbone patterns into plywood structure. Section 3.2 evaluates the accuracy of the method and Section 3.3 validates the process with the herringbone pattern of i) an algae specimen "Eremosphaera viridis" and ii) *in silico* created herringbone patterns. The supplementary information provides the algorithmic details used to calculate all the errors introduced from herringbone pattern measurements. The significance of the results are included in the final conclusions.

1.1 Plywood Architectures in Nature

In this section we provide a (i) short required background on liquid crystal solid analogues that expands on the key concepts mentioned

in the introduction, (ii) define the crucially important sensitivity of arced and herringbone patterns to the slicing angle mentioned in conjunction with Figure 1, and (iii) present examples of the diversity of orthogonal plywoods in Nature.

Nematic plywoods have been observed in some insect cuticles through the entire material [22] but also as an intermediate phase sandwiched between two different solid cholesteric-like phases, as in some beetles [23]. The role of this type of architectures in some insect cuticles is hypothesized to serve as the so-called "half wave plate" that changes the helicity of the incident light. When taking incisions of this type of plywood it can be observed (Figure 1 a-c) a family of parallel lines showing the preferred orientation which is homogeneous throughout the entire structure when the incision angle lies between 0 and $\pi/2$, as the incision angle approaches the upper limit the length of the projections decrease and when the lower limit is reached dots are observed instead.

Helicoidal plywoods were the first to be studied and explored by Bouligand [20] in crab cuticles made of chitin and is the most widely studied biological plywood and it can show ideal architectures but also non-ideal configurations such as the two-pitch plywood observed in endocarps of some fruits (made of cellulose)[24] and graded structures where the pitch varies longitudinally in the micron range scale as in the cuticle of some scarabs [19]. A characterization procedure based on the projections of the chiral nematic director to an incision plane has been reported [14, 21] which depends on the 2D periodicity of the arcs (L) and the maximum arc curvature κ_{max} which is found in the middle of the arcs. With these two experimentally measurable quantities (L, κ_{max}) one is capable of reconstructing the entire 3D structure based on 2D observations, thus complementing other optical techniques [18] leading to a more robust characterization of these structures. Depending on the type of plywood (ideal or non-ideal) the observed arced pattern can have constant or variable periodicity. These patterns are indifferent to rotation of the incision plane because of the helical structure shown.

Finally, orthogonal plywoods present abrupt changes in the orientation of 90º in strictly orthogonal architectures, but examples of angles in the range between 45º and 90º can also be found [22]. Other types of orthogonal arrangements have been reported such as the paired orthogonal system where a pair of adjacent layers are orthogonally oriented, but the subsequent set of pairs show a clockwise or anti-clockwise rotation [25] leading to nested arced-patterns. Orthogonal arrangements are known for providing with the necessary strength [26] and one of the functionalities of these plywoods is to preserve or control the shape of the material as in lazy tongs [22]. The arrangement of the fibrils is responsible for a balance in the load as occurs in laminated composites [27] and also of the mechanical failure behavior where the sliding of lamellae prior to the fracture of collagen fibers in mineralized and demineralized samples of fish scales occurs [28]. Reversible texture transitions from orthogonal to randomly oriented fibrils have been observed during the wound healing process in the skin of some amphibians [22]. The orthogonal plywood can be found in certain algae walls, in collagen based materials reinforced with mineral compounds in fish scales [22, 28] and in bone osteons composed of stacks of orthogonal layers of collagen fibers rolled in co-axial cylinders [8, 22, 29, 30]. Cornea is another example in which collagen fibrils are assembled in an orthogonal fashion in the corneal stroma (which composes 90% of the cornea thickness) and besides providing strength and shape control, the stroma is responsible for nearly 2/3 of the optical power of the eye [26]. Even when the plywood morphology is known to impact the material properties (mechanical, optical, etc.) these relationships are not fully understood [5], but the knowledge of the morphology of the plywoods is crucial to fully characterize these structures in order to make any progress along this line. The structure-property relations in orthogonal plywoods is an evolving area which evidently requires prior structure characterization. A list of natural cellulosic, collagen and chitin materials exhibiting orthogonal plywood organization are given in Table 1. It is noteworthy that as in the case of parallel and helical plywoods, a very specific underlying biochemistry does not seem to be necessary. Plywood transitions, such as helicoid ⇄ orthogonal have been reported [31] for acidic collagen I solutions, with higher pH promoting the former. This and other transitions form the basis of Neville's generic classification of biological fibrous composites [22] and highlight the importance of orthogonal arrangements.

Table 1 Examples of Biological Orthogonal Plywoods

Cellulose	Collagen	Chitin
Eremosphaera viridis cell wall (alga)[22, 32]	Paralvinella grasslei cuticle (annelid)[35]	Oryctes rhinoceros eggshell (beetle)[37]
[a] Tilia platyphyllos (larged-leaved linden)[33]	Pagrus major scales (fish)[28]	[a] Aeshna juncea cuticle (odonata)[38]
[a] Picea abies (Norway spruce)[34]	Outer lamellae human long bones[5, 30]	[a] Hydrocyrius colombiae cuticle (hemiptera)[39]
	Bird cornea (several species)[36]	[a] Coleoptera cuticle[39]

[a] Pseudo-orthogonal plywood observed

As in the case of helicoids, a pitch can be defined in orthogonal systems, where the pitch will be built up of 4 domains in strictly orthogonal plywoods if all the domains are of the same thickness. Projections to an oblique plane (oriented by a normal unit vector relative to an orthogonal coordinate system) produce the well-known herringbone patterns with a suitable combination of polar (ϕ) and azimuthal angle (θ), as shown in figure 1 [8, 17]. When one of the fibril orientation lies in any of the coordinate axes (i.e. fixing θ = 0º or 90º) no distinguishable pattern is observed by varying the polar angle in the incision plane but layers with dots and parallel lines are observed whose length depend on the orientation of the plane. On the other hand, the herringbone patterns are observed when rotating the incision plane with the azimuthal angle which

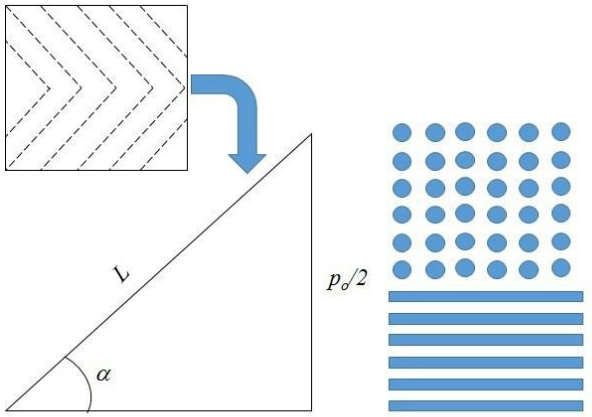

Fig. 3 Connection between the characteristic length-scale p_o of the orthogonal plywood and the projected periodicity L observed on a cross-section whose magnitude depends on the incision angle α. The upper-left frame are the observed herringbone patterns and the right shows two domains in the actual plywood.

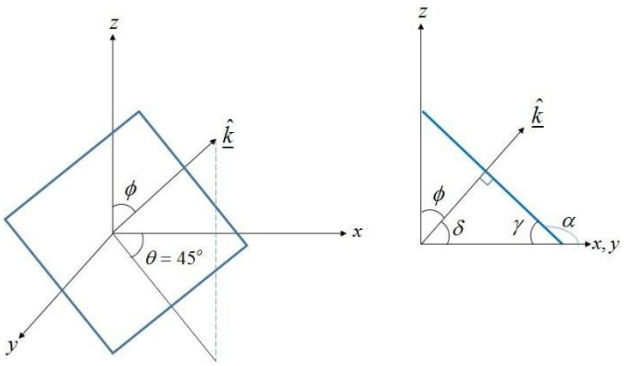

Fig. 4 (a) Schematic representation of the incision plane and the angles defining the orientation of the normal vector $\hat{k}$ in the laboratory (x,y,z) frame. (b) Side view defining the slicing angle α and the polar angle ϕ.

avoids any of the orthogonal orientation of the fibrils to coincide with the axes of the incision plane. Perfectly symmetrical herringbones are observed when the azimuthal angle takes the value of 45° i.e. the two orthogonal sets of fibrils' projection to the incision plane are of the same length because both axes of the incision plane will be shifted equally from any of the two sets of fibrils. As a consequence, any other value of θ will produce asymmetric patterns, creating the effect that any of the two sets of fibrils are longer than the other, however this is only a matter of perspective, the closer to the 45° value (i.e. the closer the ratio of both projected lengths to one) is preferred as will be shown in subsection 2.1. Even when the twist angle is fixed in these plywoods, the perspective created by projecting the fibrils of the plywood on the incision plane creates the perception that the angle between the fibrils is different from 90°, and generates the herringbone angle β (see figure 1) whose value depends on the incision angle for symmetric herringbone patterns.

2. Geometric Model

The proposed methodology is based on first sectioning a 3D plywood sample at an unknown angle (α) to obtain a 2D periodic herringbone pattern, and then measuring the pattern observables, which are the 2D periodicity L and herringbone angle β. With (L, β) we next show how to find the domain size p_o. We assume symmetric herringbone patterns unless stated otherwise, since it is always possible to obtain it by proper sectioning and it simplifies the characterization procedure.

Using simple geometry, we find the triangle that connects the plywood characteristic length p_o and the projected herringbone pattern periodicity L as shown in figure 3 leading to the following expression:

$$L = \frac{p_o}{2}\csc\alpha \tag{1}$$

Equation 1 is analogous to the one reported for helicoids [21] and as in that case it cannot be used alone to describe the orthogonal plywoods because the observed periodicity L depends on two unknown parameters α and p_o, hence additional information is required to eliminate the degree of freedom. The maximum curvature κ_{max} in the arced patterns allowed [21] closure in their characterization procedure and the herringbone angle β is expected to be the analogue parameter to the maximum curvature. Based on that hypothesis, the correspondence between the herringbone angle β and the incision angle α is obtained as follows. We set a 3D orthogonal coordinate system with unit vectors $\hat{\underline{\delta}}_x, \hat{\underline{\delta}}_y, \hat{\underline{\delta}}_z$ in which two axes lie parallel to the orientation of the two orthogonal set of parallel families of lines that represent the fibril orientation in the orthogonal plywood. The orientation of the incision plane is given by the normal vector $\hat{\underline{k}}$ pointing outwards from the plane and is a function of both the polar ϕ and the azimuthal θ angles. Figure 4 shows schematically the angles involved and how they are related to the incision plane. The projection to a given incision plane is given by extracting the tangential component of the unit vectors $\hat{\underline{\delta}}_x, \hat{\underline{\delta}}_y$ by using the projection operator defined in eqn. (2):

$$\underline{\delta}_i{}^p = (\underline{\underline{I}} - \hat{\underline{k}}\,\hat{\underline{k}}) \cdot \hat{\underline{\delta}}_i \tag{2}$$

Where the superscript "p" stands for projected and $\underline{\underline{I}}$ is the identity second order tensor with $\hat{\underline{k}} = \cos\theta\sin\phi\,\hat{\underline{\delta}}_x + \sin\theta\sin\phi\,\hat{\underline{\delta}}_y + \cos\phi\,\hat{\underline{\delta}}_z = k_x\hat{\underline{\delta}}_x + k_y\hat{\underline{\delta}}_y + k_z\hat{\underline{\delta}}_z$. By taking the dot product of the projected unit vector in the x direction with the one in the y direction (the direction of the layers in the plywood) one obtains:

$$\underline{\delta}_x{}^p \cdot \underline{\delta}_y{}^p = |\underline{\delta}_x{}^p||\underline{\delta}_y{}^p|\cos\beta = (\hat{\underline{\delta}}_x - k_x\hat{\underline{k}}) \cdot (\hat{\underline{\delta}}_y - k_y\hat{\underline{k}}) \tag{3}$$

In eqn. (3), the herringbone angle β appears automatically because it corresponds to the angle created by the projection of the unit vectors in the incision plane. Rearranging eqn. (3) in terms of the polar and azimuthal angles and by carrying out the norms of the

projected vectors, solving for β leads to:

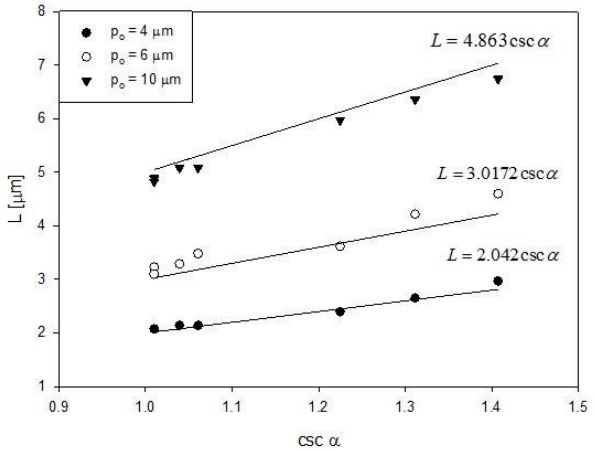

Fig. 5 Calculated herringbone pattern periodicity L as a function of csc(α) showing a linear relationship with slope $p_o/2$.

$$\cos\beta = \frac{-\sin^2\alpha\sin\theta\cos\theta}{\sqrt{1-\cos^2\theta\sin^2\alpha}\sqrt{1-\sin^2\theta\sin^2\alpha}} \quad (4)$$

Where the relationship $\phi = \pi-\alpha$ in eqn. (4) is already taken into account. Equation (4) gives an implicit relationship between α and β for a given value of θ. This was done without assuming symmetry in the herringbone patterns and is a general expression for β in terms of α and θ, however α cannot be obtained directly from this expression. One way to overcome this difficulty is to compare the projected lengths of the fibrils because as one approaches small (large) values for θ, the projected length of the fibrils aligned in the x(y) direction will decrease and the length aligned in the other direction other will increase. This is done by comparing the norm of both projected vectors as follows:

$$|\underline{\delta}^p{}_i| = \sqrt{\underline{\delta}^p{}_i \cdot \underline{\delta}^p{}_i} = \sqrt{1-k_i k_i} \quad (5)$$

The subscript "i" stands for x or y, in the case of k_i indicates the "x" or "y" component of the normal unit vector. We define the projected length ratio $\mathrm{R}(\theta,\alpha)$ as follows:

$$\mathrm{R}(\theta,\alpha) = \sqrt{\frac{1-k_x{}^2}{1-k_y{}^2}} = \sqrt{\frac{1-(\cos\theta\sin\alpha)^2}{1-(\sin\theta\sin\alpha)^2}} \quad (6)$$

Two special limit cases of this expression that do not lead to visible herringbone patterns are: i) θ = 0° and ii) θ = 90°. The ratio in the former case is restricted to the interval $0 \le R(\theta=0^o,\alpha) \le 1$ with the lower bound R=0 when the incision plane is normal to the fibrils oriented in the "x" direction and the projection of such fibrils are dots ($\alpha = 90^o$) and the higher bound R=1 when the incision plane is parallel to the fibrils, hence the projected length will be the same of the fibril ($\alpha = 0^o$). While in the latter case the ratio is within the interval $0 \le R(\theta=90^o,\alpha) < \infty$ with the lower bound when the incision plane is parallel to the fibril orientation, similarly to the higher bound of limit case i), and the higher bound when the projected length of the fibrils oriented in the "y" direction decrease to dots resulting in an indeterminate form of eqn. (6).

For the intermediate values of θ the ratio R has a finite value within $0 \le R(0<\theta<90^o,\alpha) \le 1$ and the upper bound is achieved with θ = 45°. In order to implement the procedure starting with a real orthogonal plywood specimen, one perform a sequence of cuts, recording R, until an essentially symmetric herringbone pattern is observed, which corresponds to R=1 and θ = 45°. Equation (4) now gives:

$$\cos\beta = \frac{-\sin^2\alpha}{1+\cos^2\alpha} \quad (7)$$

It is worth noting the herringbone angle β now depends only on α and is not associated with another length-scale from the sample or the incision plane. This is a consequence of the constant twist angle between the plywoods layers and is just a matter of perspective. In partial summary, the proposed methodology relies on eqns. (1) and (7) when R=1 and consists of the following steps:

1) An oblique incision giving a symmetric herringbone patterns is obtained.
2) Measure L and β from the herringbone pattern on the incision plane.
3) Calculate the incision angle α from eqn. (7).
4) Estimate the pitch p_o of the plywood using eqn. (1).
5) If the pitch is composed of 4 identical layers the average thickness of each layer can be calculated by dividing $p_o/4$.

Next we evaluate the accuracy and characterize the sensitivity of this structure reconstruction method using synthetic herringbones and then validate the method with a real biological plywood.

3. Results and Discussion

3.1 Pitch Determination

Firstly, to test the general validity of the procedure we used the Mayavi visualization software [40] where we specified the director field of an orthogonal plywood, performed oblique sections at known incision angles (α) with fixed azimuthal angle of 45° and measured the 2D periodicity L_m as a function of the known angle α. This was done for several values of p_o. Figure 5 shows the linear relationship between L_m and csc(α) extracted from the *in silico* created herringbone patterns which shows the slope to be essentially $p_o/2$ as expressed in eqn. (1).

Equation 1 shows that the pitch is undefined when α = 0 and L → ∞. Physically this means that the incision is made in one of the planes of the parallel oriented layers and no herringbone pattern is expected which could be equivalent to an infinitely large herringbone pattern since there is no change in the orientation in this layer. This is supported by eqn. (7) that predicts β = 0. As the incision angle increases the periodicity L decreases until it reaches the value $p_o/2$ which occurs when $\alpha = \pi/2$. In this limit case the periodic structure that could be anticipated is one with periodicity $p_o/2$, however $\beta = \pi$ is predicted from eqn. (7) and no herringbone pattern is visible and one might incorrectly assume the sample has the structure of a frozen nematic phase. For experimental purposes incision angles close to these limiting values are not recommended since they could lead to wrong

conclusions.

It is worth noting that incisions made at the supplementary angle

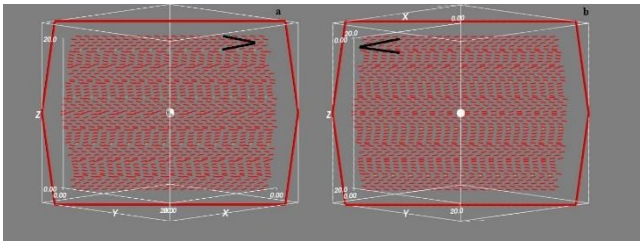

Fig.6 Herringbone patterns for a plywood with p_o = 8 μm showing the effect of the specular reflection when the incision angle is a fixed angle (α) and another incision is taken at the supplementary incision angle (b).

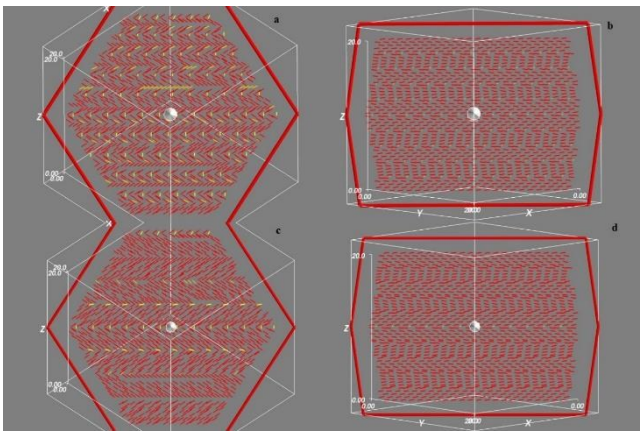

Fig. 7 In silico created herringbone patterns for a plywood of p_o = 4 (a-b) and 10 (c-d) μm, showing the effect of the periodicity with the incision angle by changing the pitch (a & c with α = 130.32°) and (b & d with α = 98.05°). The herringbone angle obtained from different plywoods at the same incision angle is equal.

π−α lead to the same periodicity and the herringbone patterns appear as their mirror image. This can be observed in figure 6 and has also been reported for helicoids [21, 24] and is consistent with goniometric studies.

3.2 Error Sensitivity on Structure Determination

In this section we provide guidelines on how to avoid procedures that yield poor predictions on the values of the length scale p_o when working with real orthogonal plywoods. In order to analyze the predictions and assess the errors of the methodology several incisions of the same plywood would be required, however this information is not easily available. Alternatively the samples showing the 2D periodic herringbone patterns can be created *in silico* with the 3D visualization tool Mayavi [40] where the director field of an orthogonal plywoods is completely specified along with p_o. Any incision plane can be quickly realized, thus allowing the total control of α. This analysis is independent of θ because R = 1. The algorithmic procedures and mathematical details are given in the supplementary information and here we emphasize the significance of the results. In this section we refer to two different sets of variables resulting from the Mayavi visualizations where the inputs for creating the synthetic herringbone patterns are the director fields with different pitch (4, 6 and 10 μm). On the one hand we have the known inputs for Mayavi p_o^M and α^M. These two variables allow the calculation of L_c^M with eqn. (1) and β_c^M with eqn. (7).

On the other hand we have the variables than can be measured from the 2D synthetic herringbone patterns which will emulate a real experimental application of the methodology: L_m and β_m. using eqn. (7) we calculate the incision angle (α_c) and finally by using eqn. (1) the pitch can be computed (p_{oc}). The former set of variables will be taken as the predictions from the model as exact values and will be compared with the latter set that simulates the application of the procedure, allowing to calculate the following relative errors since the input is known (see ESI):

$$\varepsilon_\beta = \frac{abs(\beta_c^M - \beta_m)}{\beta_c^M} * 100; \quad \varepsilon_L = \frac{abs(L_c^M - L_m)}{L_c^M} * 100; \quad \varepsilon_{p_o} = \frac{abs(p_o^M - p_{oc})}{p_o^M} * 100 \qquad (8)$$

As shown below, ε_{p_o} is more sensitive to errors in L than errors in β. The *in silico* herringbone patterns for the plywoods with p_o of 4 and 10 μm are shown in figure 7 with two different incision angles α = 130.32° (a & c) and 98.05° (b & d), the third value of the methodology is not shown for brevity but the predictions are given in tables 2 and 3. It can be seen that at least qualitatively the herringbone angle β for a given incision angle α does not change with changes in the pitch p_o comparing fig. 7 a & b with c & d respectively. This qualitative result is confirmed quantitatively with the measurements of β shown in table 2. By moving the incision angle with a constant pitch (fig. 7 a & b for p_o = 4 μm and c & d for p_o = 10 μm), it can be observed that an angle closer to 90° leads to smaller values of L, consistent with eqn. (1) and confirmed in the measurements shown in table 3.

Table 2 shows the comparison between two sets of data of the herringbone angles, β_c^M and β_m, such values did not change when the pitch was varied, demonstrating these values are pitch-independent. The relative error ε_β is small, having its maximum values when the incision angle is close to 90°. Intermediate values of the incision angle (or its complement leading to the specular image) lead generally to smaller errors, hence to improve accuracy these angles are preferred, which furnished values of β between 40° and 80°. It is worth mentioning that a similar recommendation was given in the methodology for helicoids [14].

Once β is assessed, the incision angle was calculated (α_c) and compared to the known angle α^M, which led to a negligible error (see ESI) meaning that the incision angle calculation is not significantly affected by errors in the measurement of the herringbone angle β. Table 3 compares the two sets of data for L and p_o. The errors in the periodicity L are higher with respect to the ones obtained from the herringbone angle comparisons and is propagated to the pitch calculation leading to errors between 2 – 7% for p_o. These values can be attributed mostly to L because the negligible errors found for α, and also it is worth noting that when the error in the herringbone angle β is closest to zero for the values shown in table 3 (i.e. α = 125° with ε_β = 0.68%) the difference between ε_L and ε_{po} is the largest. As mentioned above, the pitch prediction in the methodology has two sources of errors: measurements of (i) β and (ii) L, with the latter being the most sensitive parameter in the methodology (see ESI). This indicates L should be carefully measured with high precision instruments in order to have accurate predictions from this characterization

procedure.

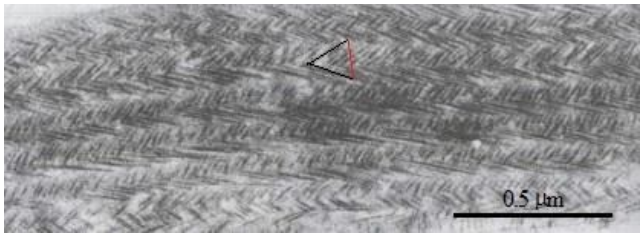

Fig. 8 Herringbone patterns observed in a sample of the alga "Eremosphaera viridis"with β = 74.3º and L = 0.1146 μm. Copyright permission (3686041171064) from Springer.

Table 2 Herringbone pattern measurements

α^M	β_m	$\beta_c{}^M$	$\varepsilon_\beta{}^b$
94.04	7.83	8.07	3.06%
98.05	16.41	15.94	2.85%
112.99	43.15	42.67	1.12%
130.32	65.00	65.81	1.24%
140.24	74.45	75.10	0.88%
151.46	82.63	82.56	0.04%
81.95	16.41	15.94	2.85%
74.21	31.65	30.45	3.79%
54.74	60.41	60.00	0.68%

[b] Error calculated as: $\varepsilon_\beta = \frac{abs(\beta_c{}^M - \beta_m)}{\beta_c{}^M} * 100$

Table 3 Pitch predictions, periodicities (measured and calculated) and errors

α	p_o = 10 μm				
	L_m	Lc^M	$\varepsilon_L{}^c$	$p_{o\,c}$	$\varepsilon_{po}{}^c$
98.05	4.89	5.05	3.20%	9.67	3.26%
125.26	5.98	6.12	2.40%	9.72	2.81%
81.95	4.82	5.05	4.46%	9.55	4.52%
	p_o = 6 μm				
	L_m	Lc^M	$\varepsilon_L{}^c$	$p_{o\,c}$	$\varepsilon_{po}{}^c$
98.05	3.23	3.03	6.50%	6.39	6.44%
125.26	3.42	3.67	6.96%	5.56	7.35%
81.95	3.09	3.03	2.29%	6.13	2.22%
	p_o = 4 μm				
	L_m	Lc^M	$\varepsilon_L{}^c$	$p_{o\,c}$	$\varepsilon_{po}{}^c$
98.05	2.08	2.02	2.81%	4.11	2.75%
125.26	2.40	2.45	2.17%	3.89	2.58%
81.95	2.08	2.02	2.81%	4.11	2.75%

[c] Errors calculated as: $\varepsilon_L = \frac{abs(L_c{}^M - L_m)}{L_c{}^M} * 100$ $\varepsilon_{p_o} = \frac{abs(p_o{}^M - p_{oc})}{p_o{}^M} * 100$

3.3 Biological Validation

The methodology was initially tested on an electron micrograph from the cell wall of the alga "Eremosphaera viridis" by calculating p_o, the average layer thickness and the cell wall thickness which is compared to the one calculated directly from the full sample. Figure 8 shows the electron micrograph of the oblique section from the cell wall of "Eremosphaera viridis" and the measured values of the herringbone angle and the periodicity of such patterns which are 74.3º and 0.1146 μm, respectively. The sample size is approximately 0.8125 μm and composed of 14 orthogonally aligned layers. Using eqns. (1) and (5) leads to the values of α = 40.74º and p_o = 0.1496μm leading to a layer thickness of 37.4 nm giving a cell wall thickness of 0.5236 μm. The cell wall thickness can also be obtained from the sample size leading to a value of 0.5303 μm which is comparable to the one obtained from the calculation of the proposed methodology (with relative error of 1.26% calculated as: $\varepsilon = \frac{abs(W_{exp} - W_{calc})}{W_{exp}}$) thus showing very good agreement with an experimental micrograph.

4. Conclusions

Biological plywoods are an important class of fibrous composites found throughout Nature and arise due to the frozen liquid crystal-like organization. Orthogonal plywoods are an important class of these materials, and are found in collagen, cellulose and chitin-based structures. In this paper we develop, apply and validate a reconstruction method for the 3D structure of orthogonal plywoods based on the geometry of 2D herringone patterns obtained by simple sectioning. The reconstruction methodology showed good agreement with experimental observations taken from oblique incisions from the alga "Eremosphaera veridis" and *in silico* created patterns. It was found that in order to have accurate predictions of domain size, moderate herringbone angles should be considered in the sample to be analyzed. Additionally, incision angles close to 0º or 90º should be avoided because incorrect predictions can be obtained. Finally, the precision in the measurement of the 2D periodicity of the herringbone pattern is the most sensitive parameter. The domain structure of orthogonal plywoods, determined from simple sectioning and the four -step algorithm presented here, lies at the core of the structure-properties relations and its determination is crucial in further biological and biomimetic developments, such as in cornea-like tissues.

Acknowledgements

This research was supported by a grand from the Natural Sciences and Engineering Council of Canada. OFAG is grateful for the financial support of CONACyT (Government of Mexico, scholarship number 313480).

Notes and references

[a] *Department of Chemical Engineering, McGill University, Montreal, Canada H3A 0C5; E-mail: alejandro.rey@mcgill.ca*

† Electronic Supplementary Information (ESI) available: [mathematical assessment in the error, error values for incision angles and flowchart of the error assessment procedure]. See DOI: 10.1039/b000000x/

1. A.D. Rey, E.E. Herrera-Valencia, *Biopolymers*, 2012, 97, 374.
2. A.D. Rey, *Soft Matter*, 2010, 6, 3402.
3. E Belamie, G Mosser, F Gobeaux, M M Giraud-Guille, *Journal of Physics: Condensed Matter*, 2006, 18, S115
4. L.Y. Li, B. Tighe, *Journal of Structural Biology*, 2006, 15, 223.
5. A. Risinger, D. Pahr, P.K. Zysset, *Proceedings of the Junior Scientist Conference*, 2010, 1, 155.
6. D. Eglin, G. Mosser, M.M. Giraud-Guille, J. Livage, T. Coradin, *Soft Matter*, 2005, 1, 129.
7. M.M. Giraud Guille, G. Mosser, C. Helary, D. Eglin, *Micron* , 2005, 36, 602.

8. P. Fratzl, M.M. Giraud-Guille: *Hierarchy in Natural Materials*. Wiley-VCH Verlag GmbH & Co. KGaA, 2011, 29.
9. Y. Murugesan, A.D. Rey, *Polymers*, 2010, 2, 766.
10. Y. Habibi, L.A. Lucia, O.J. Rojas, *Chemical Reviews*, 2010, 110, 3479.
11. *Biology of Invertebrate and Lower Vertebrate Collagen* (A Bairati and R. Garrone, ed.). NATO ASI Series, 1984.
12. F. Gobeaux, E. Belamie, G. Mosser, P. Davidson, P. Panine, M.M. Giraud-Guille, *Langmuir*, 2007, 11, 6411
13. V. Sharma, M. Crne, J.O. Park, M. Srinivasarao, *Science*, 2009, 325.
14. O.F. Aguilar Gutierrez, A.D. Rey, *Colloids and Interface Science Communications, 2014, 3, 18*
15. P. Rofouie, D. Pasini, A.D. Rey, *Colloids and Interface Science Communications*, 2014, 1, 23.
16. P. Rofouie, D. Pasini, A.D. Rey:, *Chemical Physics*, 2015.In press.
17. D. Philp, J.F. Stoddart, *Angewandte Chemie International Edition in English*, 1996, 35, 1154.
18. H. Baessler, M.M. Labes, *Molecular Crystals and Liquid Crystals*, 1969, 6, 419.
19. E. Libby, D.E. Azofeifa, M. Hernández-Jiménez, C. Barboza-Aguilar, A. Solís, I. García-Aguilar, L. Arce-Marenco, A. Hernández, W.E. Vargas, *Journal of Optics*, , 2014, 16, 082001.
20. Y. Bouligand, *Tissue and Cell*, 1972, 4, 189.
21. O.F. Aguilar Gutierrez, A.D. Rey, *Soft Matter*, 2014, 10, 9446.
22. A.C. Neville: *Biology of Fibrous Composites*. Cambridge University Press, 1993.
23. K. Allavherdyan, T. Galstian, A. Gevorgyan, R. Hakobyan, *Optics and Photonics Journal*, 2013, 3, 17.
24. J.C. Roland, D. Reis, B. Vian, B. Satiat-Jeunemaitre, M. Mosiniak, *Protoplasma*, 1987, 140, 75
25. M.M. Giraud-Guille, J. Castanet, F.J. Meunier, Y. Bouligand, *Tissue and Cell*, 1978, 10, 671.
26. S.L. Wilson, A.J. El Haj, Y. Yang, *Journal of Functional Biomaterials*, 2012, 3, 642.
27. F.C. Campbell: *Structural Composite Materials*. ASM International, 2010.
28. T. Ikoma, H. Kobayashi, J. Tanaka, D. Walsh, S. Mann, *Journal of Structural Biology*, 2003, 142, 327.
29. P. Fratzl, *Current Opinion in Colloid & Interface Science* , 2003, 8, 32.
30. M.M. Giraud Guille, *Calcified Tissue International*, 1988, 42, 167.
31. P. De Sa Peixoto, A. Deniset-Besseau, M. Schmutz, A. Anglo, C. Illoul, M.C. Schanne-Klein, G. Mosser, *Soft Matter*, 2013, 9, 11241.
32. M. Weidinger, H.G. Ruppel, *Protoplasma*, 1985, 124, 187.
33. J.C. Roland: *Cell Walls '81: Proceedings of the Second Cell Wall Meeting* (D.G. Robinson and H. Quader, ed.). Wissenschaftliche Verlagsgesellschaft, 1981.
34. N. Parameswaran, W. Liese, *Holz als Roh und Werkstoff*, 1982, 40, 144.
35. L. Lepecheux, *Biology of the Cell*, 1988, 62, 11.
36. J.L. O'donnell. *MSc. Thesis*.University of Bristol, UK, 1992.
37. P.J.S. Furneaux, A.L. Mackay: *The insect Integument* (H.R. Hepburn, ed.). Elsevier, 1976.
38. A.C. Neville: *Biology of the arthropode cuticle*. Springer-Verlag, 1975.
39. P.H. Simmons. *MSc. Thesis*. University of Bristol, UK, 1989.
40. P. Ramachandran and G. Varoquaux, *IEEE Computing in Science & Engineering*, 2011, 13, 2, 40.

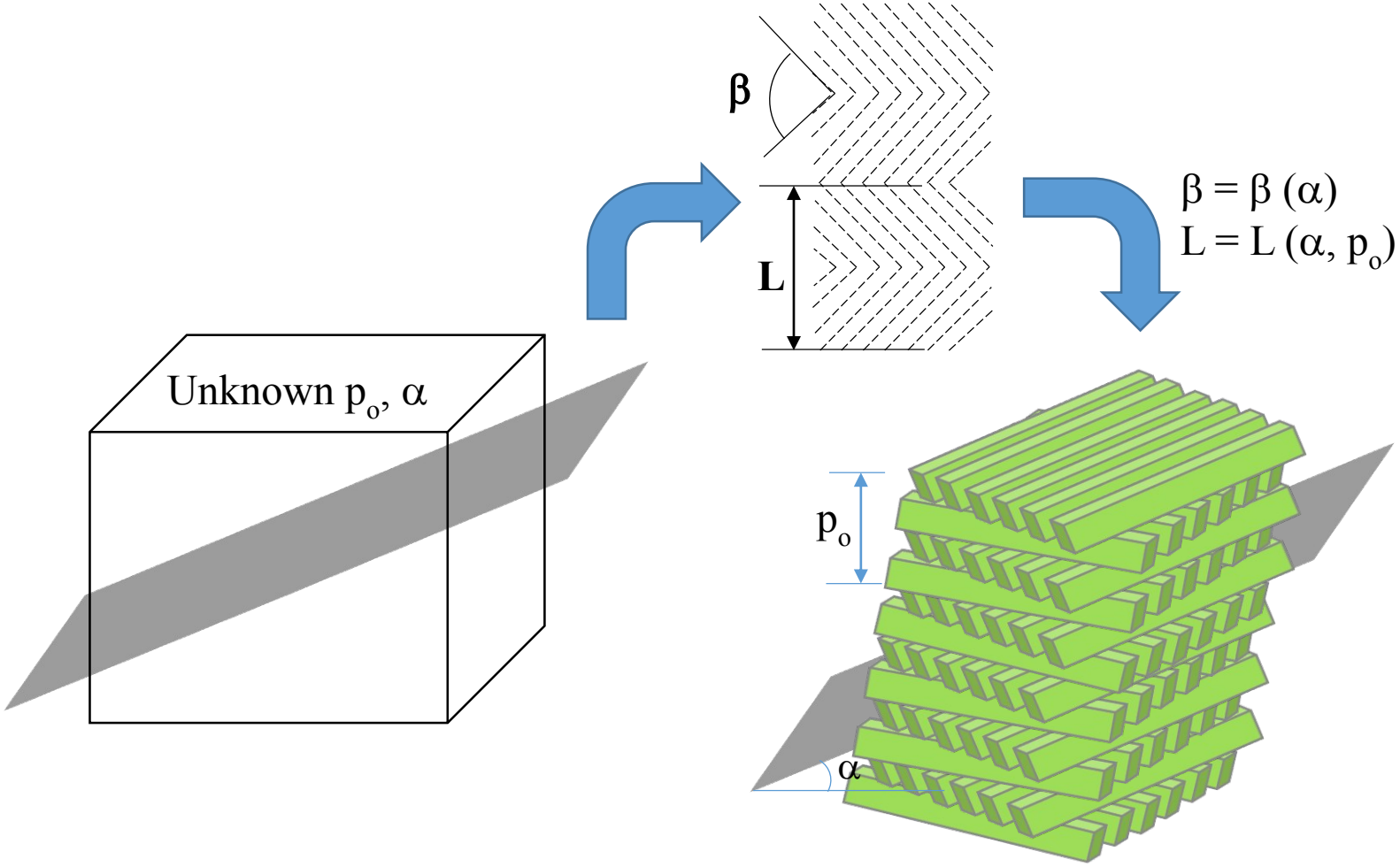

3D reconstruction procedure for orthogonal plywoods based on projected 2D herringbone patterns with error assessment and validation.